JOURNAL OF CHEMICAL INFORMATION AND MODELING

Article

pubs.acs.org/jcim

# Insights into the Role of Magnesium Triad in *myo*-Inositol Monophosphatase: Metal Mechanism, Substrate Binding, and Lithium Therapy

Shaoyong Lu,[‡,§] Wenkang Huang,[‡,§] Xiaobai Li,[‡,§] Zhimin Huang,[‡,§] Xinyi Liu,[‡,§] Yingyi Chen,[‡,§] Ting Shi,[‡,§] and Jian Zhang*[,‡,§,∥]

[‡]Department of Pathophysiology, Key Laboratory of Cell Differentiation and Apoptosis of Chinese Ministry of Education, Shanghai Jiaotong University, School of Medicine, Shanghai 200025, China

[§]Medicinal Bioinformatics Center, Shanghai Jiaotong University, School of Medicine, Shanghai 200025, China

[∥]Shanghai Key Laboratory for Tumor Microenvironment and Inflammation, Shanghai Jiaotong University, School of Medicine, Shanghai 200025, China

Supporting Information

**ABSTRACT:** *myo*-Inositol monophosphatase (IMPase) plays a pivotal role in the intracellular phosphatidylinositol cell signaling pathway. It has attracted considerable attention as a putative therapeutic target for lithium therapy in the treatment of bipolar disorder. A trio of activated cofactor $Mg^{2+}$ ions is required for inositol monophosphate hydrolysis by IMPase. In the present study, computational studies, including two-layered ONIOM-based quantum mechanics/mechanical mechanics (QM/MM) calculations, molecular modeling, and molecular dynamics (MD) simulations, were performed to ascertain the role of the $Mg^{2+}$ triad in the IMPase active site. The QM/MM calculations show that the structural identity of the nucleophilic water molecule W1 shared by $Mg^{2+}$-1 and $Mg^{2+}$-3, activated by Thr95/Asp47 dyad, is a hydroxide ion. Moreover, $Mg^{2+}$-3 needs to be conjugated with $Mg^{2+}$-1 in the binding site to create the activated nucleophilic hydroxide ion in accordance with the three-metal ion catalytic mechanism. The MD simulation of the IMPase−substrate−$Mg^{2+}$ complex shows that the three $Mg^{2+}$ ions promote substrate binding and help fix the phosphate moiety of the substrate for nucleophilic attack by the hydroxide ion. When $Mg^{2+}$-2 is displaced with $Li^{+}$, the MD simulations of the postreaction complex indicate that the conformation of the catalytic loop (residues 33 to 44) is disrupted and water molecule W2 does not coordinate with $Li^{+}$. This disruption traps the inorganic phosphate and inositolate in the active site, which lead to IMPase inhibition. By contrast, in the native $Mg^{2+}$ system, the W2 ligated by $Mg^{2+}$-2 and Asp200 aids in protonation of the leaving inositolate moiety.

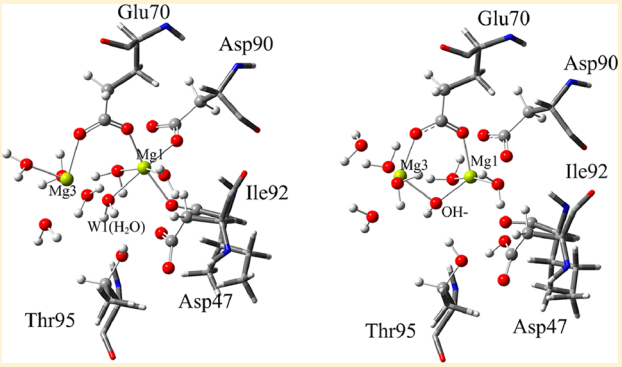


## INTRODUCTION

*myo*-Inositol monophosphatase (IMPase, EC 3.1.3.25) catalyzes the hydrolysis of several inositol monophosphate isomers to generate free *myo*-inositol. This enzymatic pathway is instrumental in the intracellular phosphatidylinositol (PtdIns) cell signaling pathway because it provides free *myo*-inositol for the biosynthesis of the key secondary messenger precursor, phosphatidylinositol 4,5-bisphosphate [PtdIns(4,5)$P_2$]. In the PtdIns cycle, receptor-activated phospholipase C hydrolyzes PtdIns(4,5)$P_2$ to produce the secondary messengers diacylglycerol and inositol 1,4,5-triphosphate [PtdIns(1,4,5)$P_3$], which activates protein kinase C and triggers the release of $Ca^{2+}$ from intracellular stores, respectively.[1−5] PtdIns(1,4,5)$P_3$ undergoes multistep hydrolysis via biphosphates to generate inositol 1-, 3-, and 4-monophosphate. The final dephosphorylation of inositol monophosphate to yield free *myo*-inositol and inorganic phosphate ($P_i$) is performed by IMPase (Scheme 1), which is activated by physiologic $Mg^{2+}$ ions and specifically inhibited by $Li^{+}$ ions, a non-native metal ion with vital functions in humans and is used to treat bipolar disorder.[6,7]

Structurally, IMPase is a homodimer of ∼30 kDa subunits, with each subunit consisting of alternating layers of $\alpha$-helix and $\beta$-sheet secondary structures organized into a penta-layered $\alpha\beta\alpha\beta\alpha$ sandwich. This $\alpha\beta\alpha\beta\alpha$ core structure consists of a total of 9 $\alpha$-helices and 13 $\beta$-strands (Figure 1) and is also extremely conserved in fructose 1,6-bisphosphatase (FBPase)[8] and inositol polyphosphate 1-phosphatase (IPPase).[9] The active site of IMPase is situated in a hydrophilic cavity lined by $\alpha_2$, $\beta_3$, $\alpha_8$, and residues 90 to 95. A $\beta$-hairpin region ($\beta_1$, Ile33-Lys36; $\beta_2$, Asp41-Thr44) is located at the entrance of the active site cavity.

Inositol monophosphate hydrolysis by IMPase was initially proposed to use a two-metal ion mechanism based on the X-ray

**Received:** April 2, 2012
**Published:** August 14, 2012





dx.doi.org/10.1021/ci300172r | *J. Chem. Inf. Model.* 2012, 52, 2398−2409

**Scheme 1. L-Inositol-1-monophosphate Hydrolysis Catalyzed by Inositol Monophosphatase**

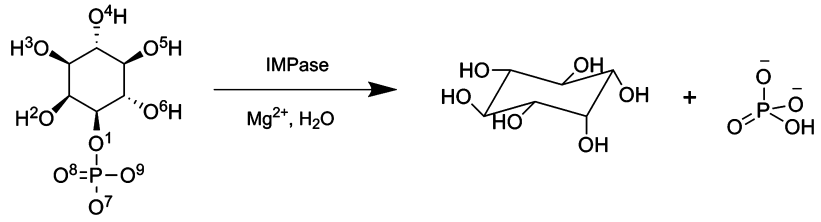


L-inositol-1-monophosphate

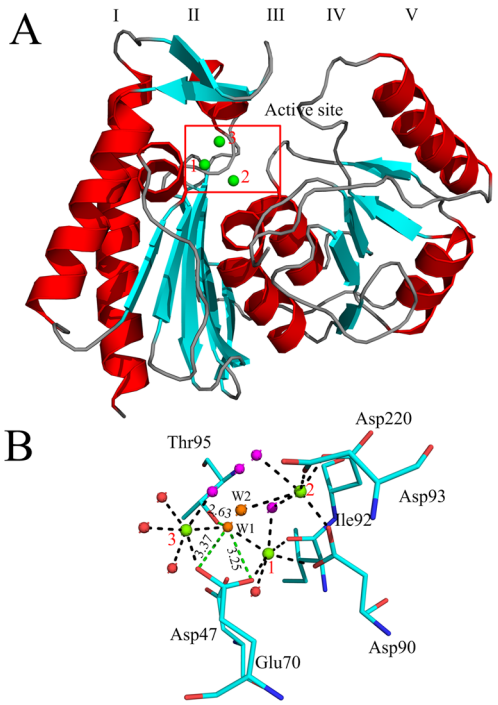


**Figure 1.** (A) A cartoon diagram of the overall folding of IMPase that depicts the penta-layered sandwich. The $\alpha$-helix, $\beta$-sheet, and loop are colored red, cyan, and gray, respectively. The three green spheres represent the three $Mg^{2+}$ ions in the active site. (B) The IMPase active site depicting the octahedral coordination of each $Mg^{2+}$ ion. The two water molecules W1 and W2 that participate in the hydrolysis are depicted as orange spheres. The four water molecules involved in modeling of the three axial phosphate O atoms and O1 of the substrate are depicted as magenta spheres. The remaining water molecules are depicted as red spheres. The $Mg^{2+}$-O coordinated interactions are shown as black dotted lines and the distances (Å) from the W1 to residues Glu70 and Thr95 are shown as green dotted lines.

structure of the enzyme in complex with $P_i$ and two $Mn^{2+}$ ions.[10] In this two-metal ion mechanism, the first $Mn^{2+}$, which is ligated by residues Glu70, Asp90, and Ile92, activates a water molecule for the nucleophilic attack on the phosphate ester. A second $Mn^{2+}$, which is ligated by residues Asp90, Asp93, and Asp220, appears to act as a Lewis acid, stabilizing the leaving inositol oxyanion. However, certain kinetic data have been difficult to explain in terms of the two-metal ion mechanism.[11−13] Recently, Gill et al. reported the first bovine IMPase structure, which was found complexed with three physiologically important $Mg^{2+}$ ions at 1.4 Å.[14] The availability of high-quality crystal structure has presented a novel opportunity for the detailed, structure-based investigation of the three-metal ion mechanism for IMPase, which also harbors general mechanistic implications for other phosphatases such as FBPase and IPPase.

More recently, available data on metal ion affinity for optimum catalysis using an archaeal IMPase determined through isothermal titration calorimetry and mobile loop mutant strongly support a three-metal ion-assisted mechanism for this IMPase.[15] Accordingly, the previously proposed two-metal ion mechanism for FBPase/IMPase was changed into a three-metal ion mechanism.[16,17]

In the IMPase active site (Figure 1B), $Mg^{2+}$ binding site 1 ($Mg^{2+}$-1) consists of the carboxylates of Glu70 and Asp90, the carbonyl of Ile92, and three water molecules. $Mg^{2+}$ binding site 2 ($Mg^{2+}$-2) consists of the carboxylates of Asp90, Asp93, Asp220, and three molecules, one of which is shared with $Mg^{2+}$-1. $Mg^{2+}$ binding site 3 ($Mg^{2+}$-3) consists of a single carboxylate of Glu70 and five water molecules, one of which is shared with $Mg^{2+}$-1. Considering $Mg^{2+}$-3 weakly interacts with IMPase, this site is only occupied at higher $Mg^{2+}$ concentrations. $Mg^{2+}$-1 and $Mg^{2+}$-2 occupy the same binding sites as the two $Mn^{2+}$ ions and act in a similar way to the two-metal ion mechanism. However, little is known about the function of $Mg^{2+}$-3 in IMPase-catalyzed inositol monophosphate hydrolysis. Additionally, whether the water molecule (W1) shared by $Mg^{2+}$-1 and $Mg^{2+}$-3 is a water molecule or a hydroxide ion is still unknown even though it has been identified as the active site nucleophile based on the structures of the substrate complexed with IMPase and the coordinates of $Mn^{2+}$ ion filling site 1 because hydrogen atoms cannot be determined under X-ray diffraction. Furthermore, if W1 is a hydroxide ion, then Glu70 or Thr95 accept a proton from W1 because they are both within its hydrogen bonding distance.

Lithium ($Li^+$), mostly as carbonate and citrate salts, is a mood stabilizer most frequently used in the treatment of bipolar disorder. Bipolar disorder, also known as manic depression, is a chronic psychiatric disorder characterized by recurrent episodes of mania and depression.[18] Experimentally, $Li^+$ inhibits IMPase *in vitro* at a $K_i$ (0.8 mM) within the therapeutic concentrations (0.5 mM to 1.5 mM) of lithium treatment for bipolar patients.[19] In this process, $Li^+$ suppressed *myo*-inositol production by inhibiting IMPase, thereby depleting the free available *myo*-inositol in brain cells and attenuating PtdIns-related signaling, which is overactive in patients with manic depression.[2] Consequently, IMPase has attracted considerable attention as a putative therapeutic target for lithium therapy in the treatment of manic depression.

Experimentally, the binding affinities of the three $Mg^{2+}$ binding sites decrease in the order $Mg^{2+}$-1 > $Mg^{2+}$-2 > $Mg^{2+}$-3.[20,21] Therefore, the low-affinity $Mg^{2+}$ binding site is presumably more susceptible to $Li^+/Mg^{2+}$ competition and is a more likely site for $Li^+$ action. Previously, a solution nuclear magnetic resonance (NMR) study by $^7Li$ indirectly confirmed that $Li^+$ replaces $Mg^{2+}$-2 in inhibiting IMPase and that inhibition by $Li^+$ is a postcatalytic event after phosphoester


dx.doi.org/10.1021/ci300172r | J. Chem. Inf. Model. 2012, 52, 2398−2409

bond cleavage in the substrate.[22] The $Mg^{2+} \rightarrow Li^{+}$ binding free energy calculations at sites 2 and 3 of the entire active site of IMPase by Dudev and Lim also show that $Li^{+}$ preferentially binds to its partially solvent-exposed $Mg^{2+}$ binding sites with a high positive charge density (+2), which indicates that $Li^{+}$ preferentially binds to site 2.[23] Despite evidence of $Li^{+}/Mg^{2+}$ competition in proteins, direct observation of $Li^{+}$ binding to the $Mg^{2+}$-2 binding site is unavailable because $Li^{+}$ only has two electrons. Thus, the protein binding of $Li^{+}$ cannot be detected using X-ray crystallography. Until recently, $^{7}Li$ magic-angle spinning solid-state NMR spectroscopy and $\{^{13}C\}^{7}Li$ dipolar recoupling experiments reported by Haimovith et al. directly detected that $Li^{+}$ binds to the $Mg^{2+}$-2 site.[24] However, the detailed mechanism by which $Mg^{2+}$-2 is dislodged by $Li^{+}$ in inhibiting IMPase is still unclear. Moreover, the three-dimensional (3D) structure of IMPase complexed with substrate or product bound in the active site, i.e., with $Mg^{2+}$ occupying the metal-binding sites, is still unavailable. Therefore, the mechanism of $Li^{+}$ inhibition and the key active site interactions between IMPase and substrate/product, as well as between $Mg^{2+}$ and substrate/product, are not fully understood. Thus, gaining insight into the enzyme structure of IMPase, particularly its active site structure and catalytic/inhibitory mechanisms, will provide a solid basis for the rational design of novel and potent IMPase inhibitors.

In the present study, computational studies that integrate own n-layer integrated molecular and orbital molecular mechanics (ONIOM)-based quantum mechanics/mechanical mechanics (QM/MM) calculations, molecular modeling, and molecular dynamics (MD) simulations were conducted to determine the function of $Mg^{2+}$ triad in the three-metal ion catalytic mechanism, substrate binding, and lithium therapy. The detailed procedures are outlined as follows: first, the IMPase active site was optimized using a two-layered QM/MM geometry to elucidate the structural identity of W1 ($H_2O$ or $OH^{-}$) and the function of $Mg^{2+}$-3 in inositol monophosphate hydrolysis. Molecular docking was then performed to dock the endogenous substrate L-inositol-1-monophosphate [L-Ins(1)P] into the active site of IMPase, and the obtained IMPase–substrate complex was examined in an MD simulation to pinpoint the structural characteristics of metal and substrate binding. Third, the $Li^{+}$-inhibited postreaction complex of the IMPase structure was modeled by displacing $Mg^{2+}$-2 and comparative MD simulations on the native $Mg^{2+}$. Alien $Li^{+}$ systems were executed to illuminate the mechanism of the inhibitory effect exerted by $Li^{+}$ on IMPase activity.

## MATERIALS AND METHODS

**QM/MM Calculations Using the ONIOM Method.** The ONIOM method[25−27] developed by Morokuma et al. was performed for QM/MM calculations as encoded in the Gaussian 03 program.[28] In the two-layered ONIOM method, the molecular system under is partitioned into an inner layer and an outer layer. The inner layer is composed of the most critical parts of the system, which involves "active-site" atoms, and is treated with accurate QM methods. The remainder of the system constitutes the outer layer, which is calculated at a low level of theory. The entire system is referred to as the "real" system and is predicted at a low level of theory.

The 1.4 Å crystal structure of IMPase complexed with three physiologic $Mg^{2+}$ ions was extracted from the RCSB Protein Data Bank (PDB code 2BJI).[14] For IMPase, the exact number of hydrogen atoms was added using the Sybyl6.8 program.[29] The heavy atoms were fixed, and the system was subjected to molecular-mechanic optimization. The W1 bridged by $Mg^{2+}$-1 and $Mg^{2+}$-3 is located far from $Mg^{2+}$-2 (4.3 Å). The main purpose for the QM/MM calculations is to determine the structural identity of W1 and the role of $Mg^{2+}$-3. Thus, the QM layer includes $Mg^{2+}$-1, $Mg^{2+}$-3, and their corresponding coordinated ligands, including six coordinated water molecules, one bridged W1, the anionic carboxymethyl group ($-CH_2-COO^{-}$) of Asp47, Glu70, and Asp90, the backbone amide group of Ile92, and the side chain methyl alcohol group ($-CH_2OH$) of Thr95, for a total of 49 atoms. The remainder was in the MM layer. Link hydrogen atoms were employed to saturate the dangling covalent bonds in the QM region. The QM layer was calculated using the density functional theory with the B3LYP method and the 6-31G* basis set. B3LYP, which comprises Becke's three-parameter hybrid gradient-corrected exchange functional,[30] incorporates the gradient-corrected correlation functional of Lee, Yang, and Parr[31] which is widely used in biomacromolecular systems.[32−34] The MM layer of the system was treated by employing the AMBER Parm96 force field, and the water molecules were described using the TIP3P model. A total of 4,895 atoms were used for the QM/MM calculations. The electrostatic interactions between the QM and MM regions were calculated using an electronic embedding scheme. The total charge of both the QM layer and the entire system was +1. Finally, the structure of the model system was fully optimized without any constraints.

**Modeling the IMPase–Substrate Complex.** Molecular docking of the endogenous substrate L-Ins(1)P to the active site of IMPase was carried out using the AutoDock4.2 software package.[35] Figure 1B shows a model of the three axial phosphate O atoms and the bridging O1 atom of the substrate. In this figure, four water molecules, which are represented by magenta balls, were deleted. Polar hydrogen atoms were added using the Hydrogen module in AutoDock Tools (ADT) for IMPase. Kollman united partial atomic charges were then assigned for the protein, and the AutoDock atom types were defined using ADT. The starting coordinates for dianionic L-Ins(1)P were extracted from the crystal structure (PDB code 1IMA),[36] supplemented with hydrogen atoms at the ideal sites on the inositol moiety and optimized for geometry. Gasteiger charges were added to the substrate, and the default root, rotatable bonds, and torsion of the substrate were set using the TORSDOF module in ADT. The grid center was defined at the centroid of the four deleted water molecules, and the number of grid points in the $x$, $y$, and $z$ directions were set to 60, 60, and 60 with a spacing value of 0.375 Å using AutoGrid. The distance-dependent function of the dielectric constant was employed to calculate the energetic maps. The Lamarckian genetic algorithm[37] was used for substrate conformational search. We used the same docking parameters as those in our previous studies.[38,39] Finally, 100 independent docking runs were conducted. The docked conformations were ranked into clusters based on the binding energy. The results were clustered using a tolerance of 1.0 Å root-mean-square deviations. The structure with the largest number of neighbors within this threshold was considered the first, largest cluster. The lowest-energy complex in the cluster with the largest number of neighbors was selected for the following MD simulation.

**Modeling the Post-Reaction Complex.** The obtained IMPase–substrate complex was used as an initial model for constructing the postreaction structure of IMPase, including IMPase, $P_i$, inositolate, and three $Mg^{2+}$ ions. The structure of

IMPase-substrate complex was superimposed with the crystal structure of yeast Hal2p PAPase−3$Mg^{2+}$−AMP−$P_i$ end-product complex (PDB code 1K9Y).[40] The coordinates of $P_i$ in 1K9Y were extracted and merged into the active site of the IMPase−substrate complex. The positions of $P_i$ and inositolate, the inositol oxyanion moiety obtained by manually breaking the P−O bond of substrate L-Ins(1)P in IMPase, were adjusted according to the $P_i$ and AMP positions of 1K9 V. Subsequently, the coordinates of L-Ins(1)P and W1 were ruled out, and the constructed initial model was further optimized using the Sybyl6.8 program.[29] The $Mg^{2+}$-2 ion was replaced with $Li^+$ in the model of the $Li^+$-inhibited IMPase structure.

**MD Simulations.** MD simulations were conducted on the these systems, namely, IMPase−3$Mg^{2+}$ (PDB code 2BJI), IMPase−3$Mg^{2+}$−L-Ins(1)P, IMPase−3$Mg^{2+}$−inositolate−$P_i$, and IMPase−2$Mg^{2+}$−$Li^+$−inositolate−$P_i$, using the program AMBER 11.[41] Default protonation states at pH 7 were set for the ionizable residues except for the residue Asp47, which was modeled as neutral. The protonation states of the histidine residues were chosen based on the results of a PROPKA calculation (http://propka.ki.ku.dk/).[42] All His residues were modeled in a neutral state. Whether HID/HIE state is selected is determined by the local hydrogen bonding network. All hydrogen atoms were added to IMPase using the Xleap tool from the AMBER suite, and the parameters were assigned according to the AMBER FF03 force field.[43] Partial atomic charges for the nonresidue atoms of hydroxide ion, inositolate, and $P_i$ were calculated using the restricted electrostatic-potential fitting protocol implemented in the ANTECHAMBER module of the AMBER 11 program and following electrostatic potential calculations at *ab initio* HF/6-31G* level. A truncated octahedral box of TIP3P waters[44] was added with a 10 Å buffer around the complex. Counterions were added to maintain electroneutrality of these systems.

To remove bad contact in the initial structures, steepest descent and conjugate gradient algorithm energy minimization methods were introduced. First, energy minimization of the water molecules and counterions with a positional restraint of 500 kcal $mol^{-1}$ $Å^{-2}$ in the complex was performed; the steepest descent method was applied for the first 2,000 steps, and then the conjugated gradient method was used for the subsequent 3,000 steps. Afterward, the entire system was minimized without any restraints; the steepest descent method was used for the first 4,000 steps, and then the conjugated gradient method was used for the subsequent 6,000 steps. After minimization, each system was heated gradually from 0 to 300 K within 50 ps. This was followed by constant temperature equilibration at 300 K for 300 ps, with a positional restraint of 10 kcal $mol^{-1}$ $Å^{-2}$ in the complex in a canonical ensemble (NVT). Finally, a 20 ns MD simulation was carried out on the IMPase−3$Mg^{2+}$−L-Ins(1)P system and 200 ns MD simulations were performed on IMPase−3$Mg^{2+}$, IMPase−3$Mg^{2+}$−inositolate−$P_i$, and IMPase−2$Mg^{2+}$−$Li^+$−inositolate−$P_i$ systems in an isothermal isobaric ensemble (NPT, $T$ = 300 K and $P$ = 1 atm) with periodic boundary conditions. An integration step of 2 fs was set for the MD simulations, and the long-range electrostatic interactions were treated using the particle mesh Ewald method[45] as well as a cubic fourth-order B-spline interpolation and by setting the direct sum tolerance to $10^{-5}$. A cutoff equal to 10 Å was used for short-range electrostatics and van der Waals interactions. The SHAKE method[46] with a tolerance of $10^{-5}$ Å was applied to constrain all covalent bonds that involve hydrogen atoms. The temperature and pressure were coupled with a time constant of 1.0 ps, isotropic position scaling, and a relaxation time of 2.0 ps according to Langevin's algorithm.[47] Coordinates were saved every 1.0 ps for analysis.

## RESULTS AND DISCUSSION

$Mg^{2+}$-1 and $Mg^{2+}$-2 operate in a similar manner as the two $Mn^{2+}$ ions involved in the two-metal ion catalytic mechanism in the IMPase active site, whereas the role of $Mg^{2+}$-3 in the three-metal ion catalytic mechanism has not been elaborated. Therefore, QM/MM calculations, as described in Materials and Methods, were performed to clarify the function of $Mg^{2+}$-3 in catalysis to supplement the three-metal ion catalytic mechanism as detected in recent experiments.

**Role of $Mg^{2+}$-3 in the Creation of Nucleophilic Hydroxide Ion.** The X-ray crystal structure of IMPase (PDB code 2BJI) shows that W1 coordinates with $Mg^{2+}$-1 and $Mg^{2+}$-3 in the active site (Figure 1B). The corresponding distances from the W1 to Glu70 OE1, OE2, and Thr95 OG atoms are 3.25, 3.37, and 2.63 Å, respectively; these values fall within the normal range for hydrogen bonding distance criteria. In addition, the hydroxyl side chain of Thr95 is hydrogen bonded to a side chain carboxylate OD2 atom of Asp47. To establish the origin of the catalytic nucleophile W1, QM/MM calculations were performed on the IMPase active site.

Figure 2 shows the optimized structure of the QM layer at the level of ONIOM (B3LYP/6-31G*:AMBER); the geometry

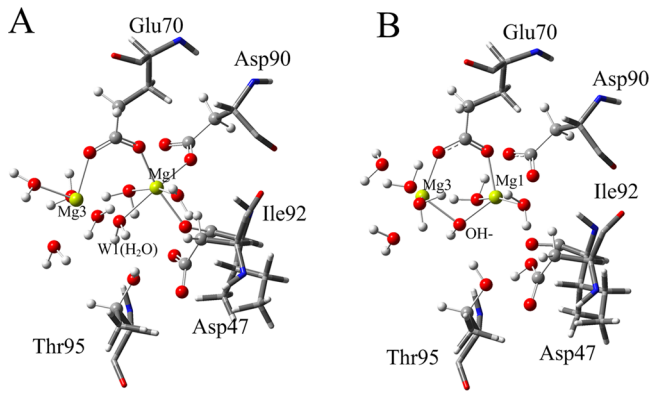


**Figure 2.** X-ray structure (A) and optimized structure (B) at the ONIOM (B3LYP/6-31G*:AMBER) level. Atoms in the QM layer are displayed as ball models.

parameters are given in Supporting Information Figure S1. QM/MM calculation reveals spontaneous proton transfer from the W1 to the oxygen atom of the hydroxyl side chain of Thr95. Synchronously, the hydrogen atom of the Thr95 side chain hydroxyl group transfers to the Asp47 side chain carboxylate OD2 atom, which then yields a hydroxide anion that coordinates with the $Mg^{2+}$-1 and $Mg^{2+}$-3 and a protonated Asp47 (Supporting Information Video S1). The emerging reactive hydroxide ion at W1 attacks the phosphorus reaction center of the substrate. A similar hydroxide ion bridged by two positively metal ions ($Zn^{2+}$ and $Mg^{2+}$) in the active site of phosphodiesterase-5 was observed in previous QM/MM studies and MD simulations.[48] The QM/MM calculation result in the present study demonstrates that the nucleophile W1 is activated by the Thr95/Asp47 dyad rather than by Glu70. This finding is highly supported by the experimental observation that mutation of the Thr95 of IMPase into Ala dramatically decreases the $k_{cat}$ 14 000-fold,[49] which is also consistent with


dx.doi.org/10.1021/ci300172r | J. Chem. Inf. Model. 2012, 52, 2398−2409

York's findings that Thr158 (corresponding to Thr95 in IMPase) of IPPase is involved in nucleophilic water activation based on kinetic data after site-directed mutagenesis.[9]

In the three-metal ion catalytic mechanism, $Mg^{2+}$-1 and $Mg^{2+}$-3 constitute a classic homobinuclear center bridged by a bidentate carboxylate of Glu70. The binding of $Mg^{2+}$-3 to IMPase is weak and noncooperative, but it is necessary for the creation of the activated nucleophile hydroxide ion. To validate this hypothesis, an additional QM/MM calculation was performed in which $Mg^{2+}$-3 was deleted, leaving W1 coordinated only by the mononuclear $Mg^{2+}$-1. Figure 3 shows

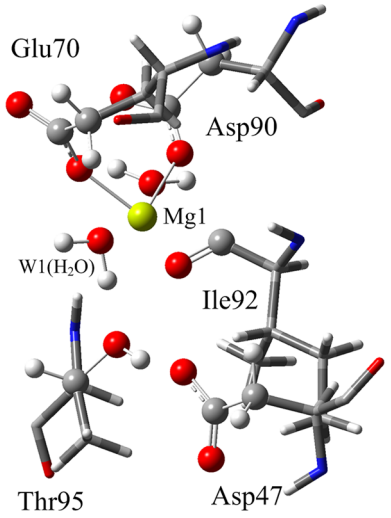


**Figure 3.** Optimized structure at the ONIOM (B3LYP/6-31G*:AMBER) level. Atoms in the QM layer are displayed as ball models.

the optimized structure of the QM layer at the ONIOM (B3LYP/6-31G*:AMBER) level. W1 cannot spontaneously transfer a proton to Thr95. Instead, W1 forms a hydrogen bond with Thr95, which, in turn, donates a hydrogen bond to Asp47. Taken together, the two QM/MM calculations show that the proton ionization of the active-site water molecule occurs more readily at the $Mg^{2+}$-1–$Mg^{2+}$-3 charged binuclear centers than the corresponding $Mg^{2+}$-1 mononuclear center. Thus, $Mg^{2+}$-3 has an appropriate configuration that further lowers the p*K*a of W1 in the creation of the hydroxide ion, which could be a candidate for the active nucleophile in the hydrolysis reaction unlike the single $Mg^{2+}$-1. This result matches well with a previous observation that a much higher $Mg^{2+}$ concentration (5 mM to 10 mM) is needed by hyperthermophile *Methanocaldococcus jannaschii* IMPase to provide the critical $Mg^{2+}$ to help create the nucleophilic hydroxide ion for optimum catalysis.[15]

**$Mg^{2+}$–Substrate and IMPase–Substrate Interactions.** As indicated above, $Mg^{2+}$-3 participates in the creation of nucleophilic hydroxide ions, and phosphate ester hydrolysis is accomplished by the direct attack of hydroxide ion on the phosphate moiety of the substrate. Consequently, the IMPase active site was further analyzed structurally because the 3D structure of the IMPase–substrate–$Mg^{2+}$ ion complex is required to understand comprehensively the structural and dynamics characteristics of the activation and inhibition mechanisms of IMPase. The enzyme, however, is active when the substrate and $Mg^{2+}$ simultaneously occupy the active site of IMPase, and the substrate would have been completely hydrolyzed before the crystal is grown.[50] Given that the crystal structure of the active IMPase–substrate–$Mg^{2+}$ complex is unavailable, an MD study was conducted with L-Ins(1)P docked into the IMPase active site to determine the structure and stability of the complex. The obtained 100 docking conformations were divided into groups based on a 1.0 Å root-mean-square deviation (rmsd) criterion using the Cluster module in ADT. The rmsd cluster analysis shows that 85 of 100 docking results significantly resemble one another, and the lowest-energy complex in this cluster was selected during MD simulation.

The RMSDs for all the C$\alpha$ atoms of IMPase and all heavy atoms of L-Ins(1)P relative to their initial minimized structure were monitored. Each frame of the trajectory is superimposed on the reference using the least-squares fit method. As shown in Figure S2, the RMSDs for IMPase and L-Ins(1)P tend to converge during the early stage of the simulation with rmsd values ~1.5 and ~0.25 Å, respectively. These findings, together with the calculations of the temperature, total energy, mass density, and volume (data not shown) during MD simulations, suggest that the system reaches equilibrium with respect to its initial structure.

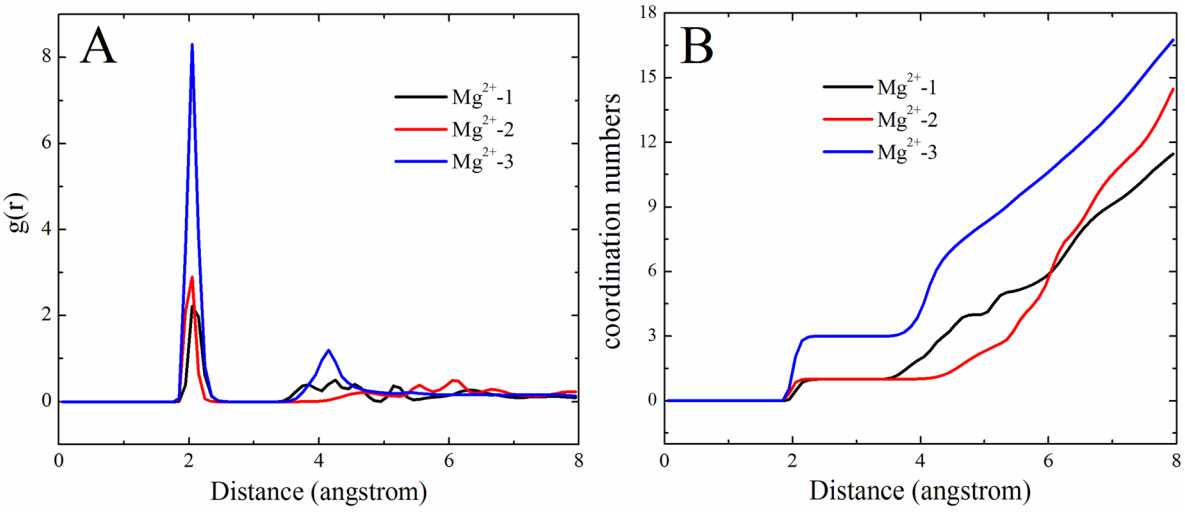


**Figure 4.** Water–metal radial distribution functions (A) and coordination numbers (B) for the $Mg^{2+}$-1 (black), $Mg^{2+}$-2 (red), and $Mg^{2+}$-3 (blue).


dx.doi.org/10.1021/ci300172r | J. Chem. Inf. Model. 2012, 52, 2398–2409

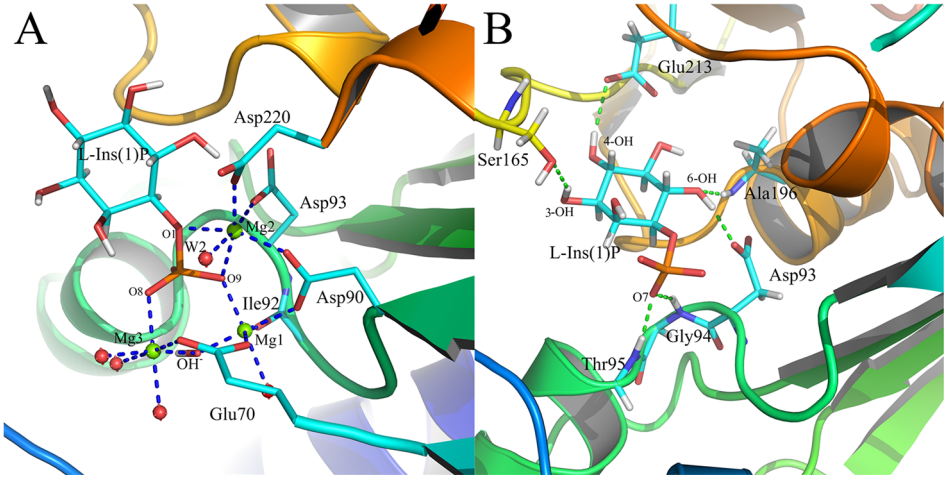


**Figure 5.** (A) The octahedral coordination of the trio of $Mg^{2+}$ ions in the active site and (B) the hydrogen bonding interactions between IMPase and L-Ins(1)P. $Mg^{2+}$ ions are depicted as green spheres, and water molecules are depicted as red spheres. Blue dotted lines and green dotted lines indicate the metal−O coordination and the hydrogen bonds, respectively.

The coordination modes around the trio of $Mg^{2+}$ ions were explored as a prototype of the cation-coordinated complexes. We first calculated the number of water molecules that coordinated with each $Mg^{2+}$ ion. Then, we computed the radial distribution function (RDF) between the $Mg^{2+}$ ions and the water molecules. Figures 4A and 4B show the RDF and coordination number (CN) derived from the MD simulation for the trio of $Mg^{2+}$ ions. As illustrated in Figure 4A (black plot), the plot shows a sharp peak centered at 2.10 Å. This peak indicates that the water molecules likely coordinated with $Mg^{2+}$-1 during the MD simulation.[51] The CN of the water molecule is 0.97 (Figure 4B, black plot), which indicates that one water molecule coordinated with $Mg^{2+}$-1. Upon close examination of the $Mg^{2+}$-1 binding site, $Mg^{2+}$-1 was found to also coordinate with the Glu70 OE1 atom, the Ile92 O atom, the Asp90 OD1 atom, the nonbridging oxygen atom O9 of L-Ins(1)P, and the oxygen atom of the nucleophilic hydroxide ion (Figure 5A). The red plots of Figures 4A and 4B show the RDF and CN that were derived from the MD simulation for $Mg^{2+}$-2. The plot shows a sharp peak centered at 2.05 Å. The CN of the water molecules was 0.98, which indicates that one water molecule (designated as W2) coordinated with $Mg^{2+}$-2. The distance between W2 and the bridging oxygen atom O1 of L-Ins(1)P was monitored and is shown in Figure S3. The calculated distance was 2.82 ± 0.10 Å, which is ideal for the protonation of the leaving inositol oxyanion after phosphoester bond cleavage. Additionally, $Mg^{2+}$-2 coordinated with the Asp90 OD2 atom, the Asp93 OD1 atom, the Asp220 OD1 atom, the nonbridging oxygen atom O9, and the bridging oxygen atom O1 of L-Ins(1)P. The blue plots in Figures 4A and 4B show the RDF and CN derived from MD simulation for the $Mg^{2+}$-3. The plot shows a sharp peak centered at 2.05 Å. The CN of the water molecules is 2.96, which indicates that three water molecules coordinated with $Mg^{2+}$-3. In addition, $Mg^{2+}$-3 coordinated with the Glu70 OE2 atom, the nonbridging oxygen atom O8 of L-Ins(1)P, and the oxygen atom of the nucleophilic hydroxide ion. Overall, the trio of $Mg^{2+}$ ions was octahedrally coordinated in accordance with the expected CNs for $Mg^{2+}$. Furthermore, based on the $Mg^{2+}$−substrate coordination modes, the trio of positively charged $Mg^{2+}$ ions coordinated with the phosphate moiety of L-Ins(1)P, neutralized its negative charge, and caused the polarization of phosphate P−O bond. This reaction enhances the electrophilic character of the phosphorus atom of L-Ins(1)P and renders the scissile phosphate more susceptible to nucleophilic attack by the negatively charged hydroxide ion. In addition, based on the crystal structure of the uncomplexed IMPase (IMPase−3$Mg^{2+}$, PDB code 2BJI), another 200 ns MD simulation was performed to estimate the mobility and residence time of the three $Mg^{2+}$ ions, as well as the mobility of the mobile loop (residues 33 to 44) in the active site of IMPase. As shown in Figure S4, when no substrate is bound to IMPase, $Mg^{2+}$-1 coordinates with the Glu70 OE1 atom, the Ile92 O atom, the Asp90 OD1 atom, and three water molecules. On the other hand, $Mg^{2+}$-2 coordinates with the Asp90 OD2 atom, the Asp93 OD1 atom, the Asp220 OD1 atom, and three water molecules. One W2 is shared by $Mg^{2+}$-1 and $Mg^{2+}$-2. $Mg^{2+}$-3 coordinates with the Glu70 OE2 atom and five water molecules. One W1 is shared by $Mg^{2+}$-1 and $Mg^{2+}$-3. Unlike the two simulated systems, the three $Mg^{2+}$ ions are stable in the active site of IMPase regardless of the presence of the substrate in the active site of IMPase. As reported by Bone et al.[10] and Ganzhorn et al.,[12] when the metals and substrate or reaction product are absent in the active site of IMPase, the mobile loop (residues 33 to 44) is highly mobile. In contrast, when the metals and substrate or reaction product bind to the IMPase, the mobile loop is less mobile. Figure S5 shows the RMSDs for the C$\alpha$ atoms of the mobile loop during the MD simulations involving the presence and absence of the substrate in the IMPase active site. The rmsd values with and without the substrate in the IMPase active site were ∼0.8 and ∼2.0 Å, respectively, which indicates that the conformation of the mobile loop without the substrate in IMPase active site is more flexible than that with the substrate in the active site of IMPase. This finding is in agreement with the published literature.

The thermodynamic stability of the trio of $Mg^{2+}$ ions can be determined from the root-mean-square fluctuation (RMSF). The calculated RMSFs for $Mg^{2+}$-1, $Mg^{2+}$-2, and $Mg^{2+}$-3 were 1.65, 1.40, and 2.47 Å$^2$, respectively, with $Mg^{2+}$-3 presenting the highest thermal parameters. This phenomenon occurred because only one protein ligand (Glu70) coordinated with $Mg^{2+}$-3. Thus, $Mg^{2+}$-3 was only occupied at higher $Mg^{2+}$ concentrations because of its weak interaction with the IMPase,

which is consistent with the experimental evidence currently available in the literature.[15]

The hydrogen bond network formed by IMPase and L-Ins(1)P was explored during the MD simulation. The formation of hydrogen bonds is characterized by the average distances between the corresponding heavy atoms and by the percentage of occurrence (Table 1). Table 1 shows that the nonbridging oxygen atom O7 of the L-Ins(1)P phosphate moiety forms two hydrogen bonds with the main chain amide groups of residues Gly94 and Thr95 (2.88 Å ± 0.11 Å, 99.80% occurrence and 3.19 Å ± 0.16 Å, 93.56% occurrence, respectively) (Figure 5B). Residues 93 to 95 form a kinked structure that encompasses the phosphate oxygen to aid in fixing the phosphate moiety for hydrolysis. In the IMPase active site, the nucleophilic hydroxide ion shared by $Mg^{2+}$-1 and $Mg^{2+}$-3 interacts simultaneously with the phosphorus atom of the phosphate moiety. The distance between the entering oxygen atom of the hydroxide ion and the phosphorus atom during MD simulation is shown in Figure S6. The calculated average distance was 2.89 ± 0.06 Å, which is strikingly shorter than the distance between the oxygen atom of substrate serine residue and the $\gamma$-phosphorus of ATP in our previous study on GSK3$\beta$/ATP/pGS (3.75 ± 0.25 Å),[52] as well as in CDK2 (3.75 ± 0.70 Å)[53] and PKA (3.80 ± 0.30 Å).[54] The dramatic decrease in the reaction coordinate distance in the IMPase system facilitates the hydrolysis reaction, which implies that IMPase is considerably active. In addition, the angles of the entering oxygen atom of the hydroxide ion, the reactive center phosphorus atom, and the leaving bridging oxygen atom O1 of L-Ins(1)P were monitored, and they are shown in Figure S7. Figure S7 shows that the calculated angle was 155.6 ± 3.6°, which suggests that the trio of $Mg^{2+}$ ions helps fix the phosphate moiety of the substrate for in-line nucleophilic attack by the hydroxide ion.

**Table 1. Summary of the Average Distances between Heavy Atoms (Å) and the Percent Occurrence of Important Hydrogen Bonding Interactions between IMPase and L-Ins(1)P**

| H-bond | X···Y | % |
|---|---|---|
| L-Ins(1)P−O7···HN-Gly94 | 2.88 ± 0.11 | 99.80 |
| L-Ins(1)P−O7···HN-Thr95 | 3.19 ± 0.16 | 93.56 |
| L-Ins(1)P$\bar{6}$−OH···OD1-Asp93 | 2.82 ± 0.14 | 97.63 |
| L-Ins(1)P$\bar{6}$-HO···HN-Ala196 | 2.94 ± 0.12 | 97.57 |
| L-Ins(1)P$\bar{4}$−OH···OE2-Glu213 | 3.02 ± 0.16 | 92.66 |
| L-Ins(1)P-3-OH···OG-Ser165 | 2.85 ± 0.19 | 50.70 |

For the inositol moiety (Table 1), the 6-hydroxyl group of L-Ins(1)P forms hydrogen bonds with the side chain of Asp93 (2.82 Å ± 0.14 Å, 97.63% occurrence) and the main chain amide group of Ala196 (2.94 Å ± 0.12 Å, 97.57% occurrence). The 4-hydroxyl group contributes a hydrogen bond to the side chain of Glu213 (3.02 Å ± 0.16 Å, 92.66% occurrence). The importance of the hydrogen bonding interactions between L-Ins(1)P and residues Asp93 and Glu213 has been confirmed by the effects of mutating either of these residues with the corresponding amide.[36] In addition, a weak hydrogen bond developed between the 5-hydroxyl group and the side chain of Ser165 during the MD simulation (2.85 ± 0.19 Å, 50.70% occurrence). Mutation of Ser165 to Ala and Ile decreased $k_{cat}/K_m$ by factors 7.0 and 3.9 for the hydrolysis of L-Ins(1)P,[36] which suggests that Ser165 is involved in the interaction with the substrate. Based on the data above, we conclude that our constructed 3D model of the IMPase−L-Ins(1)P−$Mg^{2+}$ complex is reasonable and useful in understanding the structure−function relationship in IMPase.

**Lithium Therapy Mechanism.** After obtaining a satisfactory 3D model, we investigated the lithium inhibition mechanism. First, we attempted to simulate three systems by placing $Li^+$ in each of the $Mg^{2+}$-binding sites in the 200 ns MD simulations to determine whether $Li^+$ binds with the three $Mg^{2+}$ binding sites. Figure S8 shows the last isolated snapshot from the MD trajectory for each system. The MD simulation result indicates that $Li^+$ binds with all three $Mg^{2+}$ binding sites. Careful examination of the three simulated systems indicated that when $Li^+$ binds with the $Mg^{2+}$-1 and $Mg^{2+}$-3 binding sites (Figures S8A and S8C), W2 is ligated to $Mg^{2+}$-2, which makes the W2 that protonates the leaving inositol oxyanion O1 of inositolate that leads to the release of inositol from the active site. However, when $Li^+$ binds with the $Mg^{2+}$-2 binding site (Figure S8B), W2 is not ligated to $Li^+$; thus, the leaving inositol oxyanion O1 of inositolate is not protonated, which inhibits IMPase. Furthermore, we carried out an additional ONIOM calculation where the $Mg^{2+}$-3 was replaced by $Li^+$-3 to probe whether the placement of $Li^+$ at $Mg^{2+}$-3 binding site inhibits the nucleophile creation. The remaining QM layer was the same as that in the previous homobinuclear $Mg^{2+}$-1−$Mg^{2+}$-3 ONIOM calculation, as minutely described in Materials and Methods. Figure S9 shows the optimized structure of the QM layer at the level of ONIOM (B3LYP/6-31G*:AMBER); the geometry

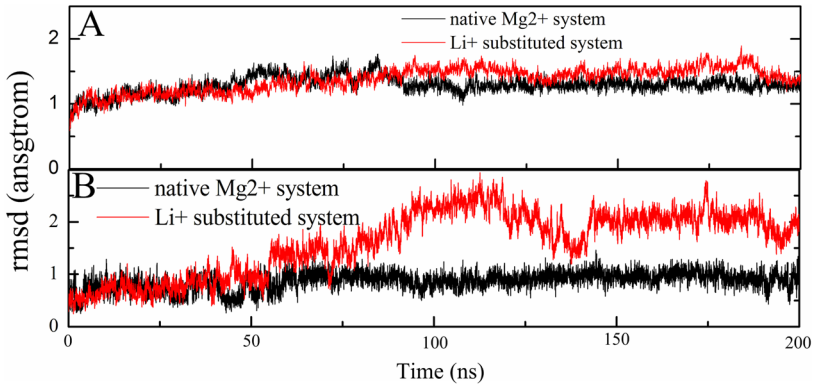


**Figure 6.** The time dependence of RMSDs relative to the X-ray crystal structure of the C$\alpha$ atoms in the entire IMPase (A) and residues 33 to 44 (B) for the native $Mg^{2+}$ system (black) and the $Li^+$ substituted system (red) in the 200 ns MD simulations.


dx.doi.org/10.1021/ci300172r | J. Chem. Inf. Model. 2012, 52, 2398−2409

parameters are given in Figure S10. As shown in Figures S9 and S10, when the $Mg^{2+}$-3 was replaced by $Li^{+}$-3, the ONIOM calculation shows that W1 cannot spontaneously transfer a proton to Thr95, leaving the water molecule coordinated to the $Mg^{2+}$-1 and $Li^{+}$-3. $Mg^{2+}$-1 is hexa-coordinated by the Glu70 OE1 atom, the Ile92 O atom, the Asp90 OD1 atom, and three water molecules. $Li^{+}$-3 is tetra-coordinated by the Glu70 OE2 atom and three molecules, one of which (W1) is shared with $Mg^{2+}$-1. The ONIOM calculation result definitely reveals that when the $Mg^{2+}$-3 was replaced by $Li^{+}$-3, the $Mg^{2+}$-1, $Mg^{2+}$-2, and $Li^{+}$-3 system was unable to create a nucleophile hydroxide ion, which further confirms the role of $Mg^{2+}$-3 in the creation of the activated nucleophile hydroxide ion.

Experimentally, inhibition of IMPase by displacing $Mg^{2+}$-2 with $Li^{+}$ is a postcatalytic event after phosphoester bond cleavage in the substrate. Therefore, we modeled the postreaction structure using the displacement of $Mg^{2+}$-2 by $Li^{+}$ based on the yeast Hal2p PAPase-3$Mg^{2+}$−AMP−$P_i$ end-product complex, as described in the Materials and Methods, which was studied using MD simulations.

The RMSDs of the native $Mg^{2+}$ and the alien $Li^{+}$ systems for all C$\alpha$ atoms in IMPase were monitored in terms of the X-ray crystal structure. As shown in Figure 6A, the rmsd value of IMPase in the native $Mg^{2+}$ system was 1.18 ± 0.13 Å. In contrast, the rmsd value of IMPase in the $Li^{+}$ substituted system was slightly higher at 1.40 ± 0.20 Å. These data show that the IMPase structure in the $Li^{+}$ substituted system underwent a conformational change compared with the IMPase in the native $Mg^{2+}$ system.[55] Thus, the average structures we calculated by averaging the coordinates from the last 100 ns of the collective trajectories for the two simulated systems. As shown in Figure 7, the superimpositions of the backbone atoms in the X-ray

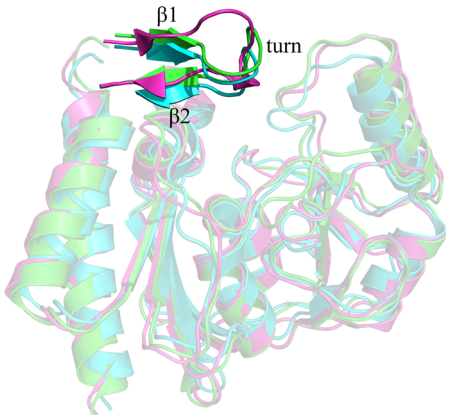


**Figure 7.** The superimpositions of the backbone atoms in the X-ray structure (green) on the average structures obtained from the MD simulations that correspond to the native $Mg^{2+}$ system (cyan) and the $Li^{+}$ substituted system (magenta).

structure on the average structures of the native $Mg^{2+}$ system and the $Li^{+}$ substituted system clearly reveal that the most significant difference occurred in secondary structures of the mobile loop, including the $\beta$-hairpin region ($\beta_1$, Ile33-Lys36; $\beta_2$, Asp41-Thr44) and the turn region (Ser37-Ala40). These structures as located at the entrance of the active site cavity where two regions in the $Li^{+}$ substituted system were displaced outwardly from the active site cavity that underwent incorrect folding. Figure 6B shows the RMSDs of the C$\alpha$ atoms of residues Ile33 to Thr44 during the MD simulations for the two systems. The RMSDs values for the native $Mg^{2+}$ system and the $Li^{+}$ substituted system were 0.80 ± 0.12 Å and 2.01 ± 0.21 Å, respectively, which indicate that the conformation of residues Ile33 to Thr44 in the $Li^{+}$ substituted system changed. Furthermore, secondary structure analyses were carried out on residues Ile33 to Thr44 during the MD simulations using the defined secondary structure of proteins (DSSP) method.[56] The secondary structure profile of residues Ile33 to Thr44 for the two systems are shown in Figure 8. The initial turn secondary structure of IMPase in the native $Mg^{2+}$ system was clearly converted into an $\alpha$-helical structure in the $Li^{+}$ substituted system after ∼10 ns of MD simulation. Moreover, the $\beta$-hairpin structure was also disrupted in the $Li^{+}$ substituted system compared with the native $Mg^{2+}$ system. Close examination of the residues in the mobile loop shows that the side chain of Lys36 in the mobile loop of the $Li^{+}$ substituted system pointed toward the bulk solvent, whereas the Lys36 in the native $Mg^{2+}$ system was directed toward the enzyme active site and interacts with residues Glu70 and Glu71 via salt bridges (Figure 9). Figure S11 shows the distance between the Lys36 nitrogen atom NZ and the two oxygen atoms OE2 of Glu70 and OE1 of Glu71 for the two simulated systems along the 200 ns MD simulations. During the simulation, the distance between the nitrogen atom NZ of Lys36 and the OE2 of Glu70 and OE1 of Glu71 in the native $Mg^{2+}$ system fluctuated at around 2.9 Å, which indicates the presence of stable salt bridges among Lys36, Glu70, and Glu71. By contrast, in the $Li^{+}$ substituted system, the distances fluctuated at around 10 Å, which indicates the absence of salt bridges among Lys36, Glu70, and Glu71. Experimentally, replacing Lys36 with Gln and Leu reduces the catalytic activity.[12,49] Ganzhorn et al.[12] explained this phenomenon based on the interaction of Lys36 with the Glu70 carboxyl group, which reduces the negative charge to which the metal ions ($Mg^{2+}$-1 and $Mg^{2+}$-3) are exposed. Consequently, the interaction should increase the polarizing potential and facilitate the deprotonation of the water nucleophile. Adversely, the mutation of Lys36 or the disruption of the salt bridges among Lys36, Glu70, and Glu71 would decrease the polarizing effect on $Mg^{2+}$-1 and $Mg^{2+}$-3 ions and prevent the efficient deprotonation of the metal-bound water nucleophile. Similar to the report by Choe et al.,[16] the conformation of the catalytic mobile loop (residues 32−44) is involved in the positioning of the third $Mg^{2+}$ ion, the transmission of the AMP allosteric signal, and the inhibition of FBPase. Thus, the conformational change of residues Ile33 to Thr44 in the $Li^{+}$ substituted system of IMPase reduced the catalytic activity.

$Li^{+}$ inhibited the IMPase activity by replacing $Mg^{2+}$-2 in the active site. Therefore, we mainly focused on the key features of metal binding characteristics at site 2. A detailed inspection of the MD trajectory was performed using the VMD program.[57] Figures 10A and 10B show the last isolated snapshot from the MD trajectory of the native $Mg^{2+}$ system and the $Li^{+}$ substituted system, respectively. The MD simulation results show that in the native $Mg^{2+}$ system, $Mg^{2+}$-2 octahedrally coordinated with the Asp90 OD2 atom, the Asp93 OD1 atom, the Asp220 OD1 atom, the oxygen atom O9 of $P_i$, the leaving inositol oxyanion O1 of inositolate, and W2. The separation between W2 and $Mg^{2+}$-2 in the postreaction complex was 2.88 ± 0.36 Å, which differs with the separation of the reactant complex (2.03 ± 0.07 Å). This difference suggests that W2 weakly coordinated with $Mg^{2+}$-2 in the postreaction complex. Additionally, analysis of the hydrogen bonding interaction

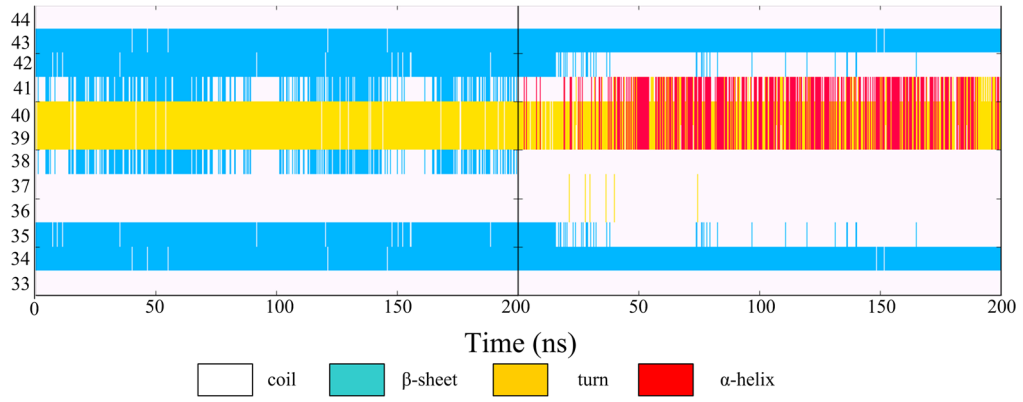


**Figure 8.** Secondary structures as a function of time for residues 33 to 44 in the native $Mg^{2+}$ system (A) and the $Li^{+}$ substituted system (B) as calculated using DSSP.

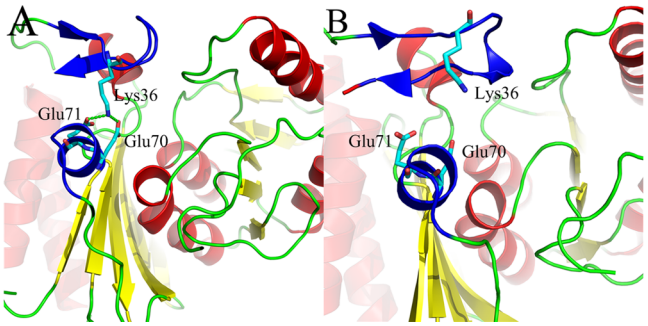


**Figure 9.** The salt bridge interactions among residues Lys36, Glu70, and Glu71 in the native $Mg^{2+}$ system (A) and in the $Li^{+}$ substituted system (B). The $\alpha$-helix, $\beta$-sheet, and loop are colored red, yellow, and green, respectively, with the two surface protein segments residues 33 to 44 and 70 to 79 in blue. Residues Lys36, Glu70, and Glu71 are displayed in stick mode. Green dashes indicate the salt bridge interactions among residues Lys36, Glu70, and Glu71.

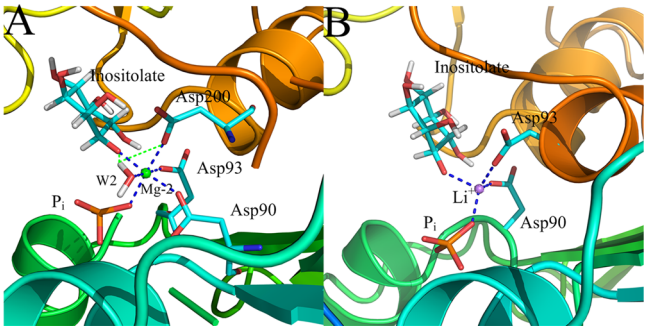


**Figure 10.** Coordination modes for the $Mg^{2+}$-2 and $Li^{+}$ in the native $Mg^{2+}$ system (A) and the $Li^{+}$ substituted systems (B). Blue dashes and green dashes indicate metal−O coordination and hydrogen bonds, respectively.

indicated that W2 donated a hydrogen bond to Asp200. Furthermore, W2 was the only source of protons near the leaving inositol oxyanion O1 of inositolate. Taken together, these findings indicate that W2 is an ideal candidate for the protonation of the leaving inositol moiety, which leads to the release of inositol from the active site. However, in the $Li^{+}$ substituted system, $Li^{+}$ tetrahedrally coordinated with the Asp93 OD1 atom, the Asp220 OD1 atom, the oxygen atom O9 of $P_i$, and the leaving inositol oxyanion O1 of inositolate. These results are consistent with the data from the Cambridge Structural Database, where the most favored CNs for $Mg^{2+}$ and $Li^{+}$ were six and four, respectively. Accordingly, we calculated the distance between W2 and $Li^{+}$ during the MD simulation. As shown in Figure S12, after ~3.8 ns of MD simulation, W2 was not ligated to $Li^{+}$, and it moved into the solvent. Thus, the leaving inositol moiety was not protonated in the $Li^{+}$ substituted system, thereby trapping $P_i$ and inositolate in the active site, which leads to IMPase inhibition. To support this notion, Wilkie et al.[58] reportedly designed nonhydrolyzable inhibitors based on substrate analogues using a bulky group approach that dislodged the W2 position in the active site resulting in IMPase inhibition.

## CONCLUSIONS

The role of the $Mg^{2+}$ triad in metal mechanism, substrate binding, and lithium therapy in IMPase was systematically delineated using computational studies, including two-layered ONIOM-based QM/MM calculations, molecular modeling, and MD simulations. QM/MM geometry optimization showed that the nucleophile W1 shared by $Mg^{2+}$-1 and $Mg^{2+}$-3 is a hydroxide ion and the spontaneous proton transfer from W1 to Thr95 and from this residue to Asp47. Furthermore, $Mg^{2+}$-3 plays an essential role in lowering the p*K*a of W1 during the creation of the hydroxide ion, which is a potential active nucleophile in the hydrolysis reaction that is not achievable by a single $Mg^{2+}$-1. These computational results provided additional evidence for the three-metal ion−assisted catalysis.

The MD simulation of IMPase−L-Ins(1)P complex revealed that the three $Mg^{2+}$ ions octahedrally coordinated with the corresponding ligands at the active site. $Mg^{2+}$-1 coordinated with the Glu70 OE1 atom, the Ile92 O atom, the Asp90 OD1 atom, the nonbridging oxygen atom O9 of L-Ins(1)P, the oxygen atom of nucleophile hydroxide ion, and one water molecule. $Mg^{2+}$-2 coordinated with the Asp90 OD2 atom, the Asp93 OD1 atom, the Asp220 OD1 atom, the nonbridging oxygen atom O9, the bridging oxygen atom O1 of L-Ins(1)P, and one water molecule W2. $Mg^{2+}$-3 coordinated with the Glu70 OE2, the nonbridging oxygen atom O8 of L-Ins(1)P, the oxygen atom of nucleophile hydroxide ion, and three water molecules. Given that $Mg^{2+}$-3 has a weaker interaction with the IMPase compared with $Mg^{2+}$-1 and $Mg^{2+}$-2, a higher root-mean-square atomic fluctuation was observed. Thus, a higher $Mg^{2+}$ concentration was required to occupy $Mg^{2+}$-3, which is consistent with previous experiments. Overall, the three $Mg^{2+}$ ions contributed to substrate binding and helped fix the phosphate moiety of the substrate for nucleophilic attack by the


dx.doi.org/10.1021/ci300172r | J. Chem. Inf. Model. 2012, 52, 2398−2409

hydroxide ion. In addition, analyses of the hydrogen bonding interaction revealed that the substrate phosphate moiety forms two hydrogen bonds with the main chain amide groups of residues Gly94 and Thr95. The 6-hydroxyl group forms hydrogen bonds with the Asp93 side chain and the main chain amide group of Ala196, and the 4-hydroxyl group contributes a hydrogen bond to the Glu213 side chain.

The MD simulations of postreaction complex indicated that in the native $Mg^{2+}$ system, W2 acts as an ideal proton donor of the leaving inositol moiety. By contrast, when $Li^{+}$ replaced $Mg^{2+}$-2, the conformational change in the catalytic loop (residues 32 to 44) was disrupted. Specifically, W2 moved into the solvent and could not coordinate with $Li^{+}$. Thus, the leaving inositol moiety remains unprotonated, thereby trapping the inositolate and $P_i$ in the active site and inhibiting IMPase. The results obtained from present computational studies are valuable in understanding the role of $Mg^{2+}$ triad in IMPase and the structure of the IMPase active site, as well as provides insights into the structural and dynamic features of other phosphatases.

## ■ ASSOCIATED CONTENT

### Ⓢ Supporting Information

The video shows the proton transfer from the W1 to Thr95 and from Thr95 to Asp47. The figures show the optimized distances at the ONIOM level, the RMSDs of IMPase and L-Ins(1)P, the distance between W2 and the bridging oxygen atom O1 of L-Ins(1)P, the angle for the entering oxygen atom of the hydroxide ion, the coordination modes for the three metal ions with and without the substrate in the IMPase active site, the RMSDs for the C$\alpha$ atoms of the mobile loop with and without the substrate, the reactive center phosphorus atom and the bridging oxygen atom O1 of L-Ins(1)P, the distance between the hydroxide ion and the phosphorus atom, the distance between W2 and $Li^{+}$ in the MD simulations, the coordination modes for the three metal ions as $Li^{+}$ binds with the three $Mg^{2+}$ binding sites, and the distances between the NZ atom of Lys36 and two oxygen atoms OE2 of Glu70 and OE1 of Glu71 during the simulation. This material is available free of charge via the Internet at http://pubs.acs.org.

## ■ AUTHOR INFORMATION

### Corresponding Author

*Phone: +86-21-63846590-776922. Fax: +86-21-64154900. E-mail: jian.zhang@sjtu.edu.cn.

### Notes

The authors declare no competing financial interest.

## ■ ACKNOWLEDGMENTS

This work was partly supported by grants from the National Basic Research Program of China (973 Program) (2011CB504001), the National Natural Science Foundation of China (21002062), the Program for Professor of Special Appointment (Eastern Scholar) at Shanghai Institutions of Higher Learning, and the Shanghai PuJiang Program (10PJ406800).

## ■ REFERENCES

(1) Berridge, M. J.; Irvine, R. F. Inositol phosphates and cell signalling. *Nature* **1989**, *341*, 197−205.
(2) Berridge, M. J.; Downes, C. P.; Hanley, M. R. Lithium amplifies agonist-dependent phosphatidylinositol responses in brain and salivary glands. *Biochem. J.* **1982**, *206*, 587−595.
(3) Berridge, M. J.; Downes, C. P.; Hanley, M. R. Neural and developmental actions of lithium: a unifying hypothesis. *Cell* **1989**, *59*, 411−419.
(4) Nishizuka, Y. The role of protein kinase C in cell surface signal transduction and tumor promotion. *Nature* **1984**, *308*, 693−698.
(5) Kishimoto, A.; Takai, Y.; Mori, T.; Kikkwa, U.; Nishizuka, Y. Activation of calcium and phospholipid-dependent protein kinase by diacylglycerol, its possible relation to phosphatidylinositol turnover. *J. Biol. Chem.* **1980**, *255*, 2273−2276.
(6) Majerus, P. W. Inositol phosphate biochemistry. *Annu. Res. Biochem.* **1992**, *61*, 225−250.
(7) Atack, J. R. Inositol monophosphatase, the putative therapeutic target for lithium. *Brain Res. Rev.* **1996**, *22*, 183−190.
(8) Ke, H. M.; Thorpe, C. M.; Seaton, B. A.; Marcus, F.; Lipscomb, W. N. Molecular structure of fructose-1,6-bisphosphatase at 2.8-Å resolution. *Proc. Natl. Acad. Sci. U.S.A.* **1989**, *86*, 1475−1479.
(9) York, J. D.; Ponder, J. W.; Chen, Z.-W.; Matthews, F. S.; Majerus, P. W. Crystal structure of inositol polyphosphate 1-phosphatase at 2.3-Å resolution. *Biochemistry* **1993**, *32*, 1844−1857.
(10) Bone, R.; Frank, L.; Springer, J. P.; Atack, J. R. Structural studies of metal binding by inositol monophosphatase: Evidence for two-metal ion catalysis. *Biochemistry* **1994**, *33*, 9468−9476.
(11) Strasser, F.; Pelton, P. D.; Ganzhorn, A. J. Kinetic characterization of enzyme forms involved in metal ion activation and inhibition of *myo*-inositol monophosphatase. *Biochem. J.* **1995**, *307*, 585−593.
(12) Ganzhorn, A. J.; LePage, P.; Pelton, P. D.; Strasser, F.; Vincendon, P.; Rondeau, J.-M. The contribution of lysine-36 to catalysis by human myo-inositol monophosphatase. *Biochemistry* **1996**, *35*, 10957−10966.
(13) Ganzhorn, A. J.; Chanal, M. C. Kinetic studies with myo-inositol monophosphatase from bovine brain. *Biochemistry* **1990**, *29*, 6065−6071.
(14) Gill, R.; Mohammed, F.; Badyal, R.; Coates, L.; Erkine, P.; Thompson, D.; Cooper, J.; Gore, M.; Wood, S. High-resolution structure of *myo*-inositol monophosphatase, the putative target for lithium therapy. *.Acta Crystallogr., Sect. D: Biol. Crystallogr.* **2005**, *D61*, 545−555.
(15) Li, Z.; Stieglitz, K. A.; Shrout, A. L.; Wei, Y.; Weis, R. W.; Stec, B.; Roberts, M. F. Mobile loop mutations in an archaeal inositol monophosphatase; Modulating three-metal ion assisted catalysis and lithium inhibition. *Protein Sci.* **2010**, *19*, 309−318.
(16) Choe, Y. Z.; Poland, B. W.; Formm, H. J.; Honzatko, R. B. Role of a dynamic loop in cation activation and allosteric regulation of recombinant porcine, fructose-1,6-bisphosphatase. *Biochemistry* **1998**, *37*, 1141−11450.
(17) Johnson, K. A.; Chen, L.; Yang, H.; Roberts, M. F.; Stec, B. Crystal structure and catalytic mechanism of the MJ0109 gene product: A bifunctional enzyme with inositol monophosphatase and fructose 1,6-bisphosphatase activities. *Biochemistry* **2001**, *40*, 618−630.
(18) Christopher, J. P.; Peter, S. K. Molecular targets of lithium action. *Annu. Rev. Pharmacol. Toxicol.* **2001**, *41*, 789−813.
(19) Hallcher, L. M.; Sherman, W. R. The effects of lithium ion and other agents on the activity of myo-inositol-1-phosphatase from bovine brain. *J. Biol. Chem.* **1980**, *255*, 10896−10901.
(20) Brocard, J. B.; Rajdev, S.; Reynolds, I. J. Glutamate-induced increases in intracellular free $Mg^{2+}$ in cultured cortical neurons. *Neuron* **1993**, *11*, 751−757.
(21) Johnson, K. A.; Chen, L.; Yang, H.; Roberts, M. F.; Stec, B. Crystal structure and catalytic mechanism of the MJ0109 gene product: A bifunctional enzyme with inositol monophoaphatase and fructose 1,6-bisphosphatase activities. *Biochemistry* **2001**, *40*, 618−630.
(22) Leech, A. P.; Baker, G. R.; Shute, J. K.; Cohen, M. A.; Gani, D. Chemical and kinetic mechanism of the inositol monophosphatase reaction and its inhibition by Li. *Eur. J. Biochem.* **1993**, *212*, 693−704.
(23) Dudev, T.; Lim, C. Competition between $Li^{+}$ and $Mg^{2+}$ in metalloproteins: Implications for lithium therapy. *J. Am. Chem. Soc.* **2011**, *133*, 9506−9515.
(24) Haimovich, A.; Eliav, U.; Goldbourt, A. Determination of the lithium binding site in inositol monophosphatase, the putative target

for lithium therapy, by magic-angle-spinning solid-state NMR. *J. Am. Chem. Soc.* **2012**, *134*, 5647−5651.
(25) Suresh, C. H.; Vargheese, A. M.; Vijayalakshmi, K. P.; Mohan, N.; Koga, N. Role of structural water molecule in HIV protease-inhibitor complexes: A QM/MM study. *J. Comput. Chem.* **2008**, *29*, 1259−1267.
(26) Vreven, T.; Morokuma, K.; Frakas, O.; Schlegel, H. B.; Frisch, M. T. Geometry optimization with QM/MM, ONIOM, and other combined methods. I. Microiterations and constraints. *J. Comput. Chem.* **2003**, *24*, 760−769.
(27) Svensson, M.; Humbel, S.; Froese, R. D. J.; Matsubara, J.; Siber, S.; Morokuma, K. Energetics using the single point IMOMO (integrated molecular orbital+molecular orbital) calculations: Choices of computational levels and model system. *J. Phys. Chem.* **1996**, *100*, 19357−19363.
(28) Frisch, M. J.; Trucks, G. W.; Schlegel, H. B.; Scuseria, G. E.; Robb, M. A.; Cheeseman, J. R.; Montgomery, J. A., Jr.; Vreven, T.; Kudin, K. N.; Burant, J. C.; Millam, J. M.; Iyengar, S. S.; Tomasi, J.; Barone, V.; Mennucci, B.; Cossi, M.; Scalmani, G.; Rega, N.; Petersson, G. A.; Nakatsuji, H.; Hada, M.; Ehara, M.; Toyota, K.; Fukuda, R.; Hasegawa, J.; Ishida, M.; Nakajima, T.; Honda, Y.; Kitao, O.; Nakai, H.; Klene, M.; Li, X.; Knox, J. E.; Hratchian, H. P.; Cross, J. B.; Adamo, C.; Jaramillo, J.; Gomperts, R.; Stratmann, R. E.; Yazyev, O.; Austin, A. J.; Cammi, R.; Pomelli, C.; Ochterski, J. W.; Ayala, P. Y.; Morokuma, K.; Voth, G. A.; Salvador, P.; Dannenberg, J. J.; Zakrzewski, V. G.; Dapprich, S.; Daniels, A. D.; Strain, M. C.; Farkas, O.; Malick, D. K.; Rabuck, A. D.; Raghavachari, K.; Foresman, J. B.; Ortiz, J. V.; Cui, Q.; Baboul, A. G.; Clifford, S.; Cioslowski, J.; Stefanov, B. B.; Liu, G.; Liashenko, A.; Piskorz, P.; Komaromi, I.; Martin, R. L.; Fox, D. J.; Keith, T.; Al-Laham, M. A.; Peng, C. Y.; Nanayakkara, A.; Challacombe, M.; Gill, P. M. W.; Johnson, B.; Chen, W.; Wong, M. W.; Gonzalez, C.; Pople, J. A. *Guassian 03*; Gaussian, Inc.: Wallingford, CT, 2003.
(29) *Sybyl version 6.8*; Tripos Associates Inc.: St. Louis, MO, 2001.
(30) Becke, A. D. Density-functional thermochemistry. III. The role of exact exchange. *J. Chem. Phys.* **1993**, *98*, 5648−5642.
(31) Lee, C.; Yang, W.; Parr, R. G. Development of the Colle-Salvetti correlation-energy formula into a functional of the electron density. *Phys. Rev. B* **1988**, *37*, 785−789.
(32) Caballero, J.; Alzate-Moralest, J. H.; Vergara-Jaque, A. Investigation of the differences in activity between hydroxycycloalkyl N1 substituted pyrazole derivatives as inhibitors of B-Raf kinase by using docking, molecular dynamics, QM/MM, and fragment-based de novo design: Study of binding mode of diastereomer compounds. *J. Chem. Inf. Model.* **2011**, *51*, 2920−2931.
(33) Zhou, P.; Zou, J.; Tian, F.; Shang, Z. Fluorine bonding: How does it work in protein-ligand interactions? *J. Chem. Inf. Model.* **2009**, *49*, 2344−2355.
(34) Lu, S.-Y.; Jiang, Y.-J.; Zou, J.-W.; Wu, T.-X. Dissection of the difference between the group I metal ions in inhibiting GSK3$\beta$: A computational study. *Phys. Chem. Chem. Phys.* **2011**, *13*, 7014−7023.
(35) Morris, G. M.; Huey, R.; Lindstrom, W.; Sanner, M. F.; Belew, R. K.; Goodsell, D. S.; Olson, A. J. AutoDock4 and AutoDockTools4: Automated docking with selective receptor flexibility. *J. Comput. Chem.* **2009**, *30*, 2785−2791.
(36) Bone, R.; Frank, L.; Springer, J. P.; Pollack, S. J.; Osborne, S.; Atack, J. R.; Knowles, M. R.; McAllister, G.; Ragan, C. I.; Broughton, H. B.; Baker, R.; Fletcher, S. R. Structural analysis of inositol monophosphatase complexes with substrates. *Biochemistry* **1994**, *33*, 9460−9467.
(37) Srivastava, H. K.; Chourasia, M.; Kumar, D.; Sastry, G. N. Comparison of computational methods to model DNA minor groove binders. *J. Chem. Inf. Model.* **2011**, *51*, 558−571.
(38) Lu, S.-Y.; Jiang, Y.-J.; Lv, J.; Zou, J.-W.; Wu, T.-X. Role of bridging water molecules in GSK3$\beta$-inhibitor complexes: Insights from QM/MM, MD, and molecular docking studies. *J. Comput. Chem.* **2011**, *32*, 1907−1918.
(39) Lu, S.-Y.; Jiang, Y.-J.; Lv, J.; Zou, J.-W.; Wu, T.-X.; Yu, Q.-S.; Zhu, W.-L. Molecular docking and molecular dynamics simulation studies of GPR40 receptor−agonist interactions. *J. Mol. Graphics Modell.* **2010**, *28*, 766−774.
(40) Patel, S.; Martínez-Ripoll, M.; Blundell, T. L.; Albert, A. Structural enzymology of $Li^+$-sensitive/$Mg^{2+}$-dependent phosphatases. *J. Mol. Biol.* **2002**, *320*, 1087−1094.
(41) Case, D. A.; Darden, T. A.; Cheatham, T. E., III; Simmerling, C. L.; Wang, J.; Duke, R. E.; Luo, R.; Walker, R. C.; Zhang, W.; Merz, K. M.; Roberts, B. P.; Wang, B.; Hayik, S.; Roitberg, A.; Seabra, G.; Kolossvary, I.; Wong, K. F.; Paesani, F.; Vanicek, J.; Liu, J.; Wu, X.; Brozell, S. R.; Steinbrecher, T.; Gohlke, H.; Cai, Q.; Ye, X.; Wang, J.; Hsieh, M.-J.; Cui, G.; Roe, D. R.; Mathews, D. H.; Seetin, M. G.; Sagui, C.; Babin, V.; Luchko, T.; Gusarov, S.; Kovalenko, A.; Kollman, P. A. *AMBER 11*; University of California: San Francisco, 2010.
(42) Bas, D. C.; Rogers, D. M.; Jensen, J. H. Very fast prediction and rationalization of PKa values for protein-ligand complexes. *Proteins: Struct., Funct., Bioinf.* **2008**, *73*, 765−783.
(43) Duan, Y.; Wu, C.; Chowdhury, S.; Lee, M. C.; Xiong, G.; Zhang, W.; Yang, R.; Cieplak, P.; Luo, R.; Lee, T. A point-charge force field for molecular mechanics simulations of proteins. *J. Comput. Chem.* **2003**, *24*, 1999−2012.
(44) Jorgensen, W. L.; Chandrasekhar, J.; Madura, J. D.; Impey, R. W.; Klein, M. L. Comparison of single potential function for simulating liquid water. *J. Chem. Phys.* **1983**, *79*, 926−935.
(45) Darden, T.; York, D.; Pedersen, L. Particle mesh Ewald: an N log(N) method for Ewald sums in large systems. *J. Chem. Phys.* **1993**, *98*, 10089−10094.
(46) Ryckaert, J. P.; Ciccotti, G.; Berendsen, H. J. C. Numerical integration of the cartesian equations of motion of a system with constraints: Molecular dynamics of n-alkanes. *J. Comput. Phys.* **1977**, *23*, 327−341.
(47) Wu, X.; Brooks, B. R. Self-guided Langevin dynamics simulation method. *Chem. Phys. Lett.* **2003**, *381*, 512−518.
(48) Xiong, Y.; Lu, H.-T.; Zhan, C.-G. Dynamics structures of phosphodiesterase-5 active site by combined molecular dynamics simulations and hybrid quantum mechanical/molecular mechanical calculations. *J. Comput. Chem.* **2008**, *29*, 1259−1267.
(49) Pollack, S. J.; Knowles, M. R.; Atack, J. R.; Broughton, H. B.; Ragan, C. I.; Osborne, S. A.; McAllister, G. Probing the role of metal ions in the mechanism of inositol monophosphatase by site-directed mutagenesis. *Eur. J. Biochem.* **1993**, *217*, 281−287.
(50) Atack, J. R.; Broughton, H. B.; Pollack, S. J. Structure and mechanism of ionsitol monophosphatase. *FEBS Lett.* **1995**, *361*, 1−7.
(51) Alzate-Morales, J. H.; Vergara-Jaque, A.; Caballero, J. Computational study on the interaction of N1 substituted pyrazole derivatives with Raf kinase: An unusual water wire hydrogen-bond network and novel interactions at the entrance of the active site. *J. Chem. Inf. Model.* **2010**, *50*, 1101−1112.
(52) Lu, S.-Y.; Jiang, Y.-J.; Zou, J.-W.; Wu, T.-X. Molecular modeling and molecular dynamics simulation studies of the GSK3$\beta$/ATP/Substrate complex: Understanding the unique P+4 primed phosphorylation specificity for GSK3$\beta$ substrates. *J. Chem. Inf. Model.* **2011**, *51*, 1025−1036.
(53) Bártová, I.; Otyepka, M.; Kříž, Z.; Koča, J. The mechanism of inhibition of the cylinc-dependent kinase-2 as revealed by the molecular dynamics study on the complex CDK2 with the peptide substrate HHASPPK. *Protein Sci.* **2005**, *14*, 445−451.
(54) Díaz, N.; Field, M. J. Insights into the phosphoryl-transfer mechanism of cAMP-dependent protein kinase from quantum chemical calculations and molecular dynamics simulations. *J. Am. Chem. Soc.* **2004**, *126*, 529−542.
(55) Huang, Z.; Zhu, L.; Cao, Y.; Wu, G.; Liu, X.; Chen, Y.; Wang, Q.; Shi, T.; Zhao, Y.; Wang, Y.; Li, W.; Li, Y.; Chen, H.; Chen, G.; Zhang, J. ASD: A comprehensive database of allosteric proteins and modulators. *Nucleic Acids Res.* **2011**, *39*, D663−D669.
(56) Kabsch, W.; Sander, C. Dictionary of protein secondary structure: pattern recognition of hydrogen-bonded and geometrical features. *Biopolymers* **1983**, *22*, 2577−2637.
(57) Humphrey, W.; Dake, A.; Schulten, K. VMD: Visual molecular dynamics. *J. Mol. Graphics* **1996**, *14*, 33−38.

(58) Wilkie, J.; Cole, A. G.; Gani, D. 3-Dimensional interactions between inositol monophosphoatase and its substrates, inhibitors and metal ion cofactors. *J. Chem. Soc., Perkin Trans.* **1995**, *1*, 2709−2727.